RSC Advances

PAPER

View Article Online
View Journal | View Issue

Cite this: *RSC Adv.*, 2025, **15**, 17675

A comprehensive study on the gemological and mineralogical characteristics and coloration mechanisms of four color varieties of natural topaz†

Xin Zhang, Nai Wang * and Yifan Gong

Topaz, a mineral with variable composition, is commonly utilized as a gemstone. Its extensive distribution and diverse coloration have attracted considerable academic interest. This study systematically investigates the mineralogical characteristics and coloration mechanisms of natural topaz with four color types (colorless, yellow, blue, and brown) by analyzing their structural features, chemical composition, and spectroscopic properties. The results indicate that the different colors of topaz arise from the substitution of Al^{3+} by impurity ions, and the presence and concentration of O^- centers. Blue topaz exhibits stable coloration through superhyperfine interactions between sufficient O^- centers and two equivalent Al^{3+}, while the concentration of O^- centers in colorless topaz is insufficient to induce coloration. Yellow topaz contains substantial Fe impurities, and the $O^{2-} \rightarrow Fe^{3+}$ charge transfer and the $^6A_{1g} \rightarrow {}^4E_g + {}^4A_{1g}$ d–d electron transitions of Fe^{3+} jointly contribute to the coloration of yellow topaz. Compared to topaz of other colors, yellow topaz exhibits a notably higher concentration of OH groups, and coupled with its coloration mechanism, we propose that the yellow coloration of topaz serves as a robust indicator of hydrothermal or metamorphic mineralization processes. Brown topaz is associated with the $^6A_{1g} \rightarrow {}^4T_{2g}$ d–d electron transitions of Fe^{3+} and a combination of trapped-electron and O^- centers. This study improves the theoretical research on natural topaz coloration mechanisms, provides comprehensive comparative analysis of the mineralogical characteristics of four color varieties of natural topaz and suggests a potential correlation between the yellow hue of topaz and its deposit genesis.

Received 23rd March 2025
Accepted 10th May 2025

DOI: 10.1039/d5ra02029h

rsc.li/rsc-advances

1 Introduction

Topaz is an aluminum silicate mineral with the general chemical formula $Al_2SiO_4(F, OH)_2$. It crystallizes within the orthorhombic crystal system and belongs to the space group *Pbnm*.[1] Fluoride ions (F^-) can be partially replaced by hydroxide ions (OH^-), but the extent of this substitution is limited. The ratio of OH to (OH + F) ranges from nearly zero to approximately thirty percent.[2] The ratio of F to OH in topaz varies with its formation temperature, which can be utilized to infer the genesis and occurrence of topaz. This variation directly influences its physical properties. For example, the refractive index of topaz is typically inversely proportional to the F content, whereas the density of topaz increases as the F content rises. When the OH content reaches a sufficient level, the structure undergoes distortion to either triclinic or monoclinic symmetry.[2,3] As shown in Fig. 1, the structure of topaz comprises isolated $[SiO_4]$ tetrahedra linked in a zigzag arrangement parallel to the *c*-axis of the crystal, along with chains of octahedra formed by $[AlO_4(F,OH)_2]$. Among the six anions surrounding each Al^{3+} ion, four are part of the $[SiO_4]$ tetrahedron, while the remaining two anions consist of either F^- or OH^- groups.[4] Topaz usually forms in granitic pegmatites and can also be found in hydrothermal vein deposits. It is an accessory mineral in fluorine-rich granitic rocks (or clastic sediments near acidic intrusive rocks) and ultrahigh-pressure rocks associated with gas–liquid or hydrothermal events.[5–7] As it is often associated with cassiterite, topaz is considered a valuable indicator of tin ore.[8]

Currently, the enhancement of color, the mechanism of coloration, and the mineral physics of topaz are focal points in scholarly research. Silva *et al.* analyzed natural and neutron-irradiated blue topaz samples using electron paramagnetic resonance and optical absorption.[9] Electron Paramagnetic Resonance (EPR) analysis of O^- centers shows superhyperfine interactions with two equivalent Al neighbors in four inequivalent positions. The O^- center concentration correlates linearly with optical absorption at 620 nm. Several studies have demonstrated, through EPR and UV-vis spectroscopy analyses, that the concentration of O^- centers in natural blue topaz is

School of Gemmology, China University of Geosciences, Beijing, 100083, China. E-mail: 2003011807@cugb.edu.cn

† Electronic supplementary information (ESI) available. See DOI: https://doi.org/10.1039/d5ra02029h

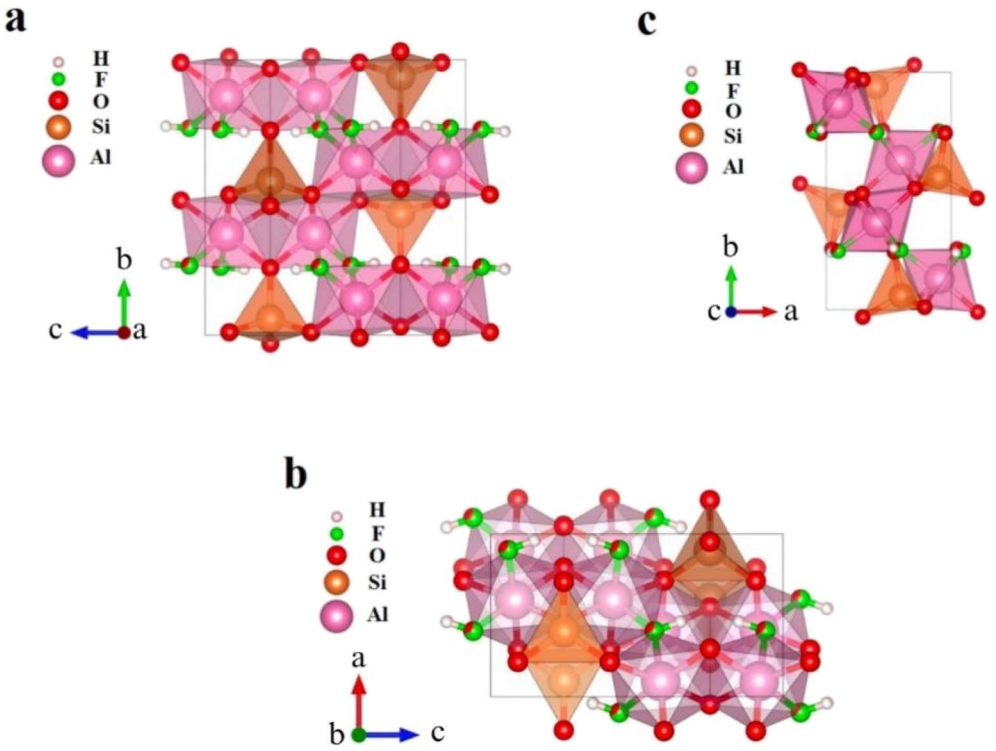

Fig. 1 (a–c) The crystal structures of topaz in the direction of three crystal axes, *a*, *b*, and *c*, respectively.

significantly higher compared to that in topaz of other colors (colorless, yellow and brown).[2,9–11] Skvortsova *et al.* indicated that the 620 nm absorption band in topaz is related to the substitution of Al^{3+} sites by Cr^{3+}, Fe^{2+} and Mn^{2+} impurity ions.[2] In addition, the broad band observed at 650 cm^{-1} in the Raman spectrum after rapid neutron irradiation may be associated with lattice disorder. Dickinson *et al.* recognized distinct EPR centers, four from impurities (two Fe^{3+}, V^{4+} and Cr^{3+}), and six from defect centers.[12] The Cr^{3+} center was identified as pink. Taran *et al.* suggested that, in addition to Cr^{3+} imparting a pink to purple hue to topaz, chromium occurs in topaz as Cr^{4+}.[13] This form of chromium is responsible for the red-orange coloration in imperial topaz. In varieties containing both Cr^{3+} and Cr^{4+}, a mixed coloration of pink and orange is observed. Song *et al.* suggested that the coloration element for yellow topaz is iron, and the OH content of yellow topaz is abnormally high.[14] In the spectroscopic studies by Pinheiro *et al.* and Londo *et al.* on topaz, yellow topaz samples showed the characteristic of having a higher OH content than colorless and blue samples.[3,15] Komatsu examined the effects of temperature and pressure on the crystal structure of topaz and discovered that as the temperature increased, the average Al–O bond distance expanded considerably, whereas the Al–F and Si–O bond distances exhibited only minor increments.[16] Correcher found that both cathodoluminescence (CL) and thermoluminescence (TL) emissions of topaz are strongly dependent on temperature.[17] Cryogenic treatments induce a significant decrease in the CL and TL intensity above 400 nm, which is associated with intrinsic OAl* defects and iron point defects. Furthermore, Correcher also confirmed the existence of a continuous trap distribution system in topaz.[17] In addition, the coloration of gem minerals is increasingly recognized as a critical geochemical tracer, offering insights into fluid compositions, redox conditions, and tectonic settings during mineral formation. For instance, in emeralds, chromophore ratios (Cr/V) distinguish metamorphic from hydrothermal origins, while tourmaline color zonation reflects evolving fluid chemistries in pegmatitic systems.[18,19] Similarly, topaz color variations may encode signatures of its genetic environment. Hydrothermal systems, characterized by fluid–rock interactions and volatile-rich conditions, often favor OH^- incorporation and trace element substitution, whereas high-temperature magmatic settings typically stabilize F-rich compositions.[7,20,21] Previous studies on the genesis types of topaz and their correlations with chemical composition have been relatively clear, but the connection between the color of topaz and genesis types has not yet been established. In addition, the understanding of the causes of the various colors in natural topaz is still not well-developed. The only unambiguous assignment is that of chromium, which causes pink and red. There is still a lack of comparative research on the spectroscopic features and coloration mechanism of natural topaz of different colors.

In this study, a total of thirteen natural topaz samples of four colors were selected. Conventional gemological tests were used to study the gemological characteristics, surface morphology and internal features of the samples. The chemical composition of the samples of different colors was characterized using X-ray fluorescence spectrometry (XRF) and electron probe

microanalysis (EPMA). The spectral characteristics and crystal structure of the samples were studied using infrared spectroscopy (IR), Raman spectroscopy (Raman) and powder X-ray diffraction (XRD). The coloration mechanism of topaz of different colors was explored using ultraviolet-visible spectrophotometer (UV-vis). This study advances the theoretical framework for understanding natural topaz coloration mechanisms and establishes a systematic experimental foundation for its gemological and mineralogical characteristics. Furthermore, we propose a novel hypothesis linking topaz color to deposit genesis, offering critical insights into the formation processes of yellow topaz.

2 Materials and methods

2.1. Materials

As presented in Fig. 2, thirteen natural topaz samples were analyzed in this study and numbered according to their colors. The samples include colorless topaz from Brazil (W-1, W-2, W-3), yellow topaz from Yaogangxian, Hunan Province, China (Y-1, Y-2, Y-3, Y-4), blue topaz from Brazil (B-1, B-2, B-3) and brown topaz from Mexico (BR-1, BR-2, BR-3), which are water-eroded pebbles with frosted surfaces. The rest of the samples are in irregular crystal forms.

2.2. Methods

Routine gemological characterization tests were performed using gemological microscopes, refractometers, electronic balances, dichroscopes, polariscopes, gemological handheld spectroscopes, and UV fluorescent lamps. Among these instruments, the handheld gemological spectrometer generates continuous spectra throughout the visible light wavelength range through dispersion, presenting the absorption and emission characteristic spectral lines of gemstones. However, its accuracy is far inferior to that of the UV-visible spectrometer.

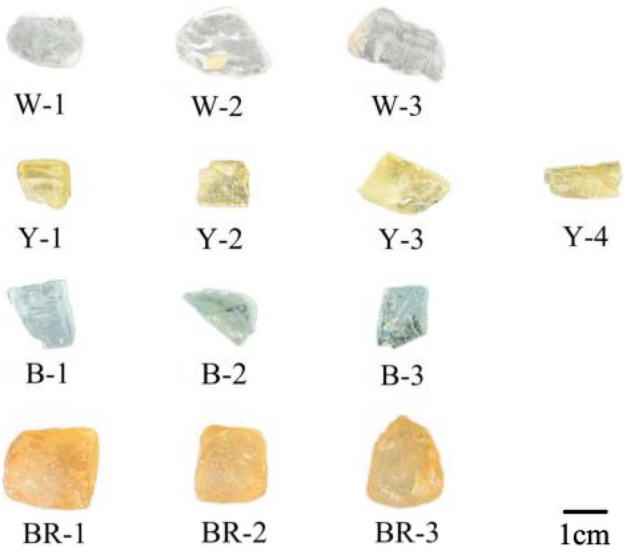

Fig. 2 A picture of the topaz samples.

Routine gemological characterization tests were conducted at the China University of Geosciences (Beijing) Gemological Experimental Teaching Center.

The composition and structure were characterized by X-ray fluorescence spectroscopy, electron probe micro-analysis and X-ray powder diffraction. The X-ray fluorescence spectra for component characterization were collected by an EDX-7000 energy spectrometer produced in Tsushima, Japan, measured at China University of Geosciences (Beijing) Gem Testing Laboratory. The experimental test conditions were an element analysis range of (13)Al–(92)U, and detection limits of 0.1%. Background correction was carried out using circular aluminum plates. The EPMA analysis was conducted using an EPMA-1720 instrument manufactured by Shimadzu, Japan. The detection limit was set at 500 ppm, and the test conditions included an accelerating voltage of 15 kV, a current of 10 nA, and an electron beam spot diameter of 5 μm, measured at China University of Geosciences (Beijing) Geoscience Test Center. The X-ray powder diffraction analysis for structural characterization was performed using a Smart Lab X-ray diffractometer (D8 Focus, Bruker, Germany) of the School of Materials, China University of Geosciences (Beijing, China). The instrument utilized CuKα radiation with a scanning speed of 10° per min, a scanning range of 5 to 80° and a sampling step width of 0.02°(2θ). The sample was prepared as a 300-mesh powder.

Spectroscopic characterization includes infrared spectroscopy, Raman spectroscopy, and UV-vis absorption spectroscopy. The remaining spectroscopic tests were all performed at the Gem Testing Laboratory, the School of Gemmology, China University of Geosciences (Beijing). Infrared spectroscopic data were acquired utilizing a TENSOR 27 Fourier transform infrared spectrometer manufactured in Germany. The measurements were conducted in reflectance mode with a spectral scanning range spanning from 400 cm^{-1} to 4000 cm^{-1}. The resolution was 2 cm^{-1}, the scan count ranged from 50 to 100, the test voltage was 220 V and the scanning speed was 10 kHz. Aluminium sheets were used for background correction. Raman spectra were acquired using an HR Evolution micro-Raman spectrometer (HORIBA, Japan). The experimental voltage was 220 V, the current was 10 A, the spectral resolution was 1 cm^{-1}, and the laser wavelength was 532 nm with a scanning range of 200–4000 cm^{-1}. Background correction was performed utilizing silicon wafers. UV-vis absorption spectra were recorded using a UV-3600 UV-vis spectrophotometer (Shimadzu, Japan). The experimental conditions were as follows: the sampling interval was 1.0 nm, the testing method was the diffuse reflection method, the measurement wavelength range was 200–800 nm, the light source conversion wavelength was 300 nm, and the grating conversion wavelength was 850 nm. Background correction was performed using a barium sulfate whiteboard.

3 Results and discussion

3.1. Basic gemological characteristics

Comprehensive conventional gemological characterization analyses were per-formed on all thirteen topaz samples (Table 1). The colorless, yellow and blue topaz samples were all

Table 1 Basic gemological characteristics of the topaz samples

Sample	W-1	W-2	Y-1	Y-2	B-1	B-2	BR-1	BR-2
Color	Colorless		Yellow		Blue		Brown	
Transparency	Transparent		Transparent		Transparent		Opaque	
Refractive index	1.614–1.624	1.615–1.624	1.621–1.629	1.620–1.629	1.619–1.628	1.620–1.628	1.616–1.625	1.62
Relative density	3.49	3.41	3.53	3.47	3.69	3.51	3.59	3.57
Polariscope	Four bright and four dark phenomena							
Spectroscope	No characteristic absorption band							
UV fluorescent lamps	Long wave: no		Long wave: no		Long wave: weak yellow-green		Long wave: no	
	Short wave: no		Short wave: weak orange-yellow		Short wave: no		Short wave: weak orange-yellow	

transparent with a vitreous luster, while the brown topaz sample was opaque. Under cross-polarized illumination, the samples undergo full rotational orientation (360°), exhibiting alternating bright and dark extinction patterns at 90° intervals, which is a uniaxial crystal heterogeneity. All topaz samples can be observed to have absorption spectra under a gemological handheld spectroscope, but they are not characteristic and cannot reflect the specific coloring elements within them, that is, they have no characteristic absorption spectra. The sample shows weak fluorescence or no fluorescence under ultraviolet light. The refractive index ranges from 1.613 to 1.631, and the refractive index of topaz samples with different colors is slightly different, with the refractive index of yellow topaz slightly larger than that of other colors. In general, the refractive index of topaz is inversely proportional to the content of F.[3] The birefringence is 0.008–0.010. The specific gravity of the topaz samples was determined to range between 3.41 and 3.69, demonstrating close alignment with the characteristic theoretical range documented for natural topaz minerals.[8]

The colorless sample has the best transparency. Under magnification, a set of complete cleavages parallel to {001} and conchoidal fractures can be observed (Fig. 3a). A yellowish-brown staining substance is observed in the near-surface regions of samples W-2 and W-3 (Fig. 3b). Parallel gas–liquid two-phase inclusions (Fig. 3c) and a large number of oriented needle-shaped inclusions (Fig. 3d) were observed inside the samples. Negative crystals can be seen inside the blue sample B-3 (Fig. 3e). The cylindrical longitudinal striations of the yellow sample Y-4 are well developed and occur in association with tourmaline (Fig. 3f). The surface of the brown sample is frosted and has poor transparency, with almost no internal features visible.

3.2. Composition and structure analysis of topaz

3.2.1. Compositional analysis based on X-ray fluorescence spectroscopy and electron probe micro-analysis. As shown in Table 2, the results of X-ray fluorescence spectroscopy show that the main elements of the topaz samples of four colors are Al, Si and O, in addition to metallic elements (Ca, Zn, Ge, K, Sr, Rb, Mo, Y), transition metal elements (Fe, Cu, Zr, Re, Ti), and non-metallic elements (Br, S). The content of the fluorine element cannot be detected using X-ray fluorescence spectroscopy, which accounts for the significant deviation of the measured

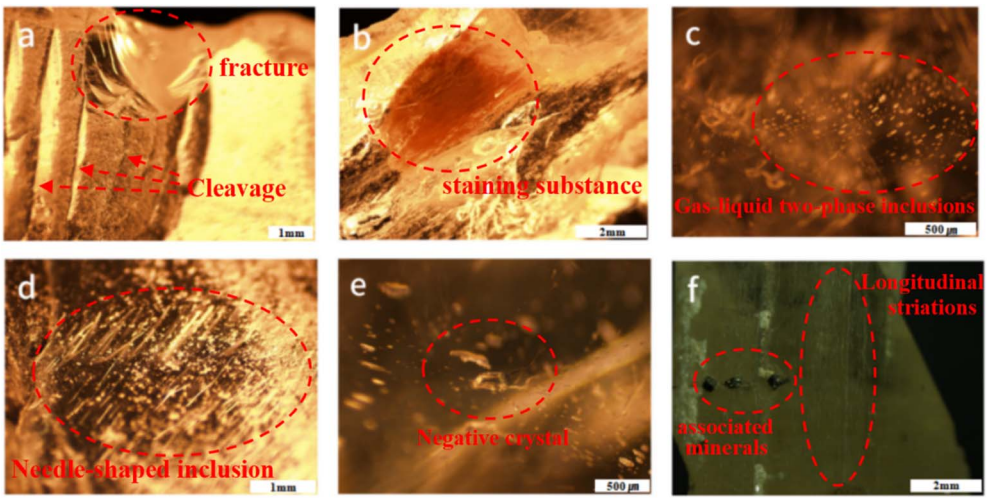

Fig. 3 Surface and internal characteristics of topaz. (a) Cleavage and fracture (W-3); (b) yellowish-brown staining substance (W-2); (c) gas–liquid two-phase inclusions (W-1); (d) a needle-shaped inclusion (W-3); (e) a negative crystal (B-3); (f) cylindrical longitudinal striations and associated minerals (Y-4).

Table 2 X-ray fluorescence spectral analysis data of the topaz samples (wt%)

	W-1	W-2	Y-1	Y-2	B-1	B-2	BR-1	BR-2
Al	51.430	50.963	49.890	49.597	50.320	50.417	50.949	51.244
Si	47.916	48.999	49.769	49.066	49.116	49.325	48.855	47.436
S	0.565	0.000	0.000	0.666	0.000	0.000	0.000	0.712
Rb	0.029	0.000	0.000	0.000	0.000	0.006	0.000	0.000
Fe	0.024	0.000	0.051	0.064	0.028	0.040	0.046	0.025
Y	0.016	0.000	0.000	0.000	0.000	0.000	0.000	0.000
Ge	0.011	0.038	0.024	0.026	0.051	0.049	0.049	0.000
Sr	0.010	0.000	0.000	0.000	0.000	0.000	0.009	0.000
Ca	0.000	0.000	0.203	0.111	0.405	0.000	0.000	0.000
Ti	0.000	0.000	0.037	0.033	0.000	0.000	0.000	0.000
Mo	0.000	0.000	0.018	0.000	0.000	0.000	0.006	0.000
Cu	0.000	0.000	0.008	0.008	0.013	0.011	0.000	0.000
K	0.000	0.000	0.000	0.381	0.000	0.000	0.000	0.000
Hf	0.000	0.000	0.000	0.048	0.000	0.000	0.000	0.000
Er	0.000	0.000	0.000	0.000	0.068	0.000	0.000	0.000
Cr	0.000	0.000	0.000	0.000	0.000	0.080	0.000	0.000
Pr	0.000	0.000	0.000	0.000	0.000	0.062	0.000	0.000
Th	0.000	0.000	0.000	0.000	0.000	0.009	0.000	0.000
Ag	0.000	0.000	0.000	0.000	0.000	0.000	0.065	0.054
Zr	0.000	0.000	0.000	0.000	0.000	0.000	0.013	0.000
Br	0.000	0.000	0.000	0.000	0.000	0.000	0.009	0.000
Re	0.000	0.000	0.000	0.000	0.000	0.000	0.000	0.529

contents of the major components Al_2O_3 and SiO_2 in topaz from their respective theoretical values of 55.4 wt% and 32.6 wt%. The average Al content of colorless topaz, yellow topaz, blue topaz and brown topaz is 50.958 wt%, 49.744 wt%, 50.369 wt% and 51.097 wt%, respectively. The average Fe content is 0.005 wt%, 0.058 wt%, 0.034 wt% and 0.036 wt%, respectively. The Al content in colorless and brown topaz is the highest, while that in yellow topaz is the lowest. However, the Fe content in yellow topaz is significantly higher than that in other colors, indicating that the substitution of Fe for Al may be closely related to the coloration mechanism of yellow topaz. In addition to Fe, Ti was exclusively detected in yellow topaz. Trace Ti^{3+}/Ti^{4+} in yellow topaz could participate in charge-balancing mechanisms during Fe^{3+} substitution for Al^{3+}, though its minimal concentration suggests a secondary role. Prior studies on aluminosilicates indicate that even minor Ti incorporation can influence defect stability or enhance charge transfer efficiency related to Fe^{3+}, which may subtly intensify the yellow coloration.[22]

We further carried out electron probe micro-analysis to clarify the differences in F content among the topaz samples of different colors and to improve the characterization of their compositional profiles. Two points were randomly selected from each sample for electron microprobe analysis, and the average value was taken as the data of that sample. As shown in Table 3, the average concentrations of Al_2O_3 and SiO_2 were 55.827 wt% and 32.387 wt%, respectively, which are in close agreement with the theoretical values. The mean F contents in the colorless, yellow, blue, and brown topaz samples were 10.587 wt%, 10.079 wt%, 10.402 wt%, and 10.276 wt%, respectively. Notably, the F content in yellow topaz is significantly lower compared to other varieties, suggesting a higher degree of OH^- substitution for F^- in yellow topaz relative to the other colors. Apart from the colorless topaz samples, the Zn element was detected in all of the other topaz samples, indicating that Zn might play a role in influencing the coloration of topaz. Although Zn^{2+} is larger than Al^{3+}, its low concentration likely prohibits its direct substitution for Al^{3+} in the crystal lattice. Instead, Zn might occupy interstitial sites or form complexes with OH^- groups, potentially stabilizing hydroxyl-rich environments, as observed in hydrothermal/metamorphic systems.[23] Nevertheless, the impact of Zn on the color of topaz is merely secondary, as its fully filled d orbitals ($3d^{10}$) are incapable of undergoing d–d electron transitions and lack the redox activity required for charge transfer. Hence, Zn cannot be regarded as a chromogenic element in gemology.

3.2.2. X-ray diffraction analysis. As illustrated in Fig. 4, the X-ray diffraction patterns obtained from colorless, yellow, blue, and brown topaz samples exhibit a high degree of alignment with the reference standard ICSD No. 59410 ($Al_2F_2SiO_4$). This correspondence strongly suggests that no significant structural discrepancies exist among topaz samples of varying coloration. Furthermore, the observed diffraction peaks display sharp and well-defined profiles, which indicates that the topaz samples have high crystallinity. As presented in Table S1 of the ESI,† all topaz diffraction peak positions exhibit a minor range of offsets and small angular deviations, which are attributed to the ratio of F to OH and the substitution of impurity elements for Al. To be specific, the minor angular deviations in the X-ray diffraction

Table 3 Electro probe micro-analysis data of the topaz samples (wt%)

Data	F	TiO_2	SiO_2	Cr_2O_3	Na_2O	V_2O_5	Cl	MnO	MgO	FeO	K_2O	ZnO	Al_2O_3	NiO	CaO	P_2O_5	Total
W-1	10.85	0.00	32.56	0.01	0.00	0.00	0.01	0.02	0.00	0.01	0.00	0.00	55.29	0.01	0.01	0.00	98.77
W-2	11.48	0.01	32.05	0.03	0.00	0.04	0.01	0.01	0.00	0.00	0.00	0.00	55.25	0.05	0.01	0.00	98.95
W-3	9.43	0.00	33.48	0.00	0.00	0.02	0.01	0.01	0.00	0.00	0.01	0.00	56.05	0.02	0.02	0.01	99.06
Y-1	10.66	0.04	32.69	0.00	0.01	0.00	0.00	0.01	0.00	0.03	0.01	0.10	55.95	0.07	0.01	0.03	99.61
Y-2	10.11	0.02	32.91	0.01	0.01	0.01	0.01	0.02	0.01	0.02	0.00	0.12	56.06	0.00	0.00	0.02	99.34
Y-3	9.47	0.01	32.45	0.01	0.01	0.00	0.00	0.01	0.00	0.01	0.01	0.03	56.77	0.02	0.01	0.00	98.80
B-1	10.12	0.02	32.07	0.01	0.01	0.02	0.01	0.00	0.00	0.02	0.01	0.05	56.68	0.02	0.01	0.02	99.08
B-2	10.05	0.02	32.58	0.01	0.01	0.01	0.01	0.01	0.00	0.03	0.00	0.00	56.32	0.03	0.01	0.05	99.15
B-3	11.04	0.07	32.30	0.01	0.00	0.00	0.00	0.00	0.01	0.04	0.00	0.03	52.84	0.02	0.01	0.01	96.38
BR-1	10.71	0.02	31.99	0.01	0.03	0.01	0.00	0.02	0.00	0.01	0.00	0.03	55.92	0.00	0.01	0.00	98.76
BR-2	9.96	0.00	32.18	0.00	0.01	0.03	0.00	0.03	0.01	0.00	0.01	0.03	56.24	0.02	0.01	0.03	98.56
BR-3	10.15	0.04	31.38	0.02	0.01	0.03	0.00	0.01	0.00	0.01	0.00	0.03	56.56	0.01	0.00	0.02	98.28

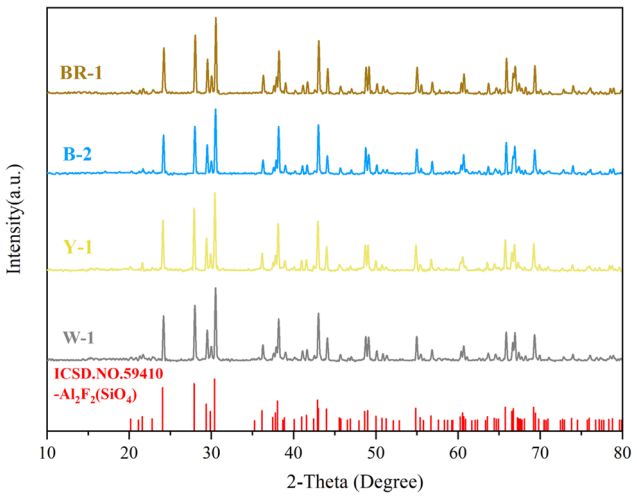

Fig. 4 X-ray diffraction patterns of topaz samples W-1, Y-1, B-2, and BR-1.

peaks arise from variations in the lattice parameters (*a*, *b*, *c*), which are influenced by F^-/OH^- substitution and impurity substitutions. Previous studies have demonstrated that the unit cell parameters *a* and *b*, as well as the unit cell volume of topaz exhibit positive linear correlations with OH content.[7] OH^- has a larger ionic radius (1.37 Å) compared to F^- (1.33 Å). Substitution of F^- by OH^- expands the lattice, increasing the d-spacing, which results in a shift of the diffraction peaks to lower 2-theta angles. Fe^{3+} has a larger ionic radius (0.645 Å) compared to Al^{3+} (0.535 Å). Fe^{3+} substituting Al^{3+} further expands the lattice, contributing to its larger cell volume and corresponding peak shifts. To obtain the unit cell parameters of topaz samples of different colors, the topaz samples underwent structural refinement using the Rietveld method. The X-ray diffraction data of the topaz samples were processed using the HighScore software. Comparing the unit cell parameters of the four color types of topaz (Table 4), the unit cell parameters *a*, *b* and *c*, and the unit cell volume of yellow topaz are significantly larger than those of the other three colors. According to the results of XRF, there are higher Fe concentrations in the yellow topaz, consequently leading to an increase in the unit cell parameters. The yellow topaz sample has a significantly larger unit cell parameter than topaz of other colors, indicating that it may contain an abnormally high OH content. This is evidenced by the minimum density of yellow topaz, as its density exhibits a decreasing trend with an increase in OH content. The blue and brown topaz exhibit greater elemental diversity relative to other color types (Table 3). This compositional complexity induces minor but measurable deviations in lattice parameters, likely attributable to synergistic interactions between trace substituent ions.

3.3. Spectroscopy analysis of topaz

3.3.1. Infrared spectra analysis. Infrared spectral data were collected using the reflection method, and the infrared spectra were plotted using Origin software from the raw data. A comparative study was conducted on the infrared spectral characteristics of topaz of different colors. As illustrated in Fig. 5, the test samples display characteristic infrared spectra of topaz that are in agreement with those documented in RRUFF database entry #R040121. To facilitate comparison and demonstration, the spectra of the four samples with the highest clarity and most intense color intensity, that is W-1, Y-1, B-1, and BR-1, were selected for presentation in the manuscript, and the infrared spectra of the other test samples are presented in Fig. S1 of the ESI.† The infrared absorption peaks were assigned according to the study by Farmer *et al.*.[24] As presented in Table S2 of the ESI,† there are five distinct infrared absorption features corresponding to different vibrational modes in topaz. The first type is the Si–O–Si antisymmetric stretching vibration, located in the range of 1200–900 cm^{-1}, with specific peak positions at 989, 932, and 914 cm^{-1}. The second type is the Al–O stretching vibration, located at 900–720 cm^{-1}, with a specific peak at 895 cm^{-1}. The third type is the Si–O symmetrical stretching vibration, located around 715 cm^{-1}. It is noteworthy that in the 600–1200 cm^{-1} spectral region, the bending and stretching modes of the –OH group are occasionally observed to coexist within the crystal structure.[25] The fourth type is the bending vibration of Al–O–Si, which is located below 587 cm^{-1}, with specific peak positions at 565, 507, 491, 474, and 426 cm^{-1}. The fifth type is the symmetrical stretching vibration of –OH, located at 3652 cm^{-1}.(ref. 26) This absorption peak is closely associated with the yellow hue of topaz, and only the yellow samples exhibit this absorption peak, which indicates that yellow topaz has an excessively high content of OH, also corresponding to the XRD results discussed in the preceding section of this paper. It is noteworthy that the bending vibration peak position of Al–O–Si in the blue topaz samples exhibits a discernible shift. This phenomenon may be attributed to the superhyperfine interaction between the O^- center in the blue topaz and the two nearest equivalent Al atoms located at the four magnetically inequivalent positions.[9]

3.3.2. Raman spectra analysis. To further characterize and compare the vibrational properties of the topaz samples of

Table 4 Crystal cell parameters of topaz samples W-1, Y-1, B-2, and BR-1

Sample number	*a* (Å)	*b* (Å)	*c* (Å)	Cell volume (Å^3)	$\alpha = \beta = \gamma$ (°)	Density (g cm^{-3})	R_{wp} (%)
W-1	8.7930	8.3868	4.6483	342.79	90	4.19	9.18
Y-1	8.8085	8.3945	4.6557	344.26	90	4.17	9.22
B-2	8.7918	8.3871	4.6475	342.70	90	4.19	9.47
BR-1	8.7866	8.3823	4.6448	342.10	90	4.19	9.06

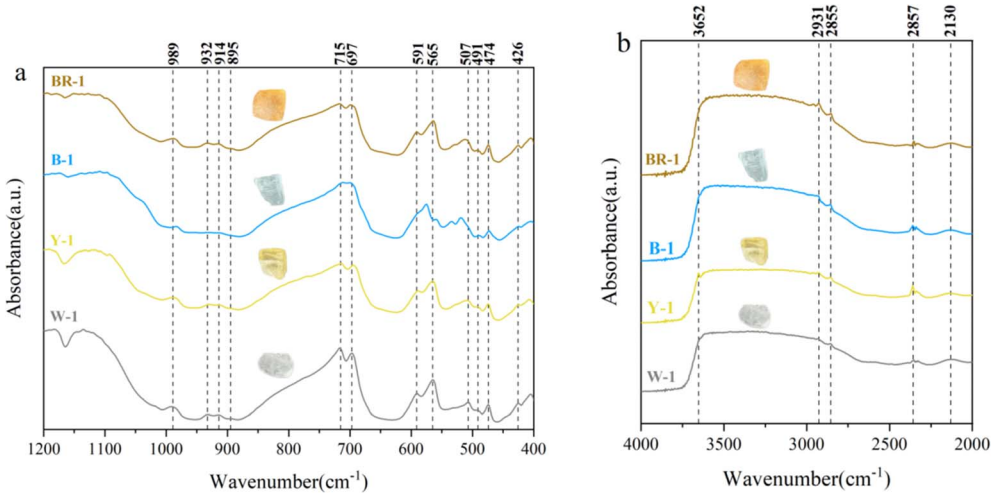

Fig. 5 (a) Infrared reflection spectra of the topaz samples (400–1200 cm^{-1}); (b) infrared reflection spectra of the topaz samples (2000–4000 cm^{-1}).

different colors, we collected Raman spectra from the four distinct color varieties of topaz (Fig. 6). Raman spectra for all samples were initially plotted from the raw data using Origin software. For the yellow topaz samples, background subtraction and Savitzky–Golay smoothing were applied to the spectral lines within the 3200–4000 cm^{-1} range prior to analysis, while the Raman data for the other samples were directly plotted without additional processing. Table S3 in the ESI† lists peak positions and assignments for the Raman spectra. The peaks at 240, 267, 287, 520, and 936 cm^{-1} are assigned to the various Si–O vibration modes in the [SiO_4] groups.[27] The vibrational bands observed in the 330–500 cm^{-1} spectral region are attributed to stretching and bending modes of [AlO_6] octahedral units, coupled to the bending modes of the [SiO_4] tetrahedra.[2] The band observed at 856 cm^{-1} arises from vibrational coupling of [SiO_4] between asymmetric and symmetric stretching modes, a phenomenon induced by hydroxyl-for-fluorine substitution within the crystal lattice.[28] The sharp peak observed at 3649 cm^{-1} corresponds to the stretching vibration of structural hydroxyl groups.[29] The analysis of the OH band profile reveals that the observed asymmetry arises from an unresolved splitting into two peaks, centered at 3639 cm^{-1} and 3647 cm^{-1}, caused by two types of physically nonequivalent F sites where the OH/F substitution can occur.[3] Four distinct peaks observed at 3412, 3795, 3893, and 3962 cm^{-1} demonstrate a direct correlation with the sample's yellow coloration, while simultaneously suggesting elevated hydroxyl concentrations within yellow topaz and the atypical position of hydroxyl groups (–OH) within the crystal structure.[30] This observation is consistent with the XRD and infrared spectroscopy results discussed earlier in this article.

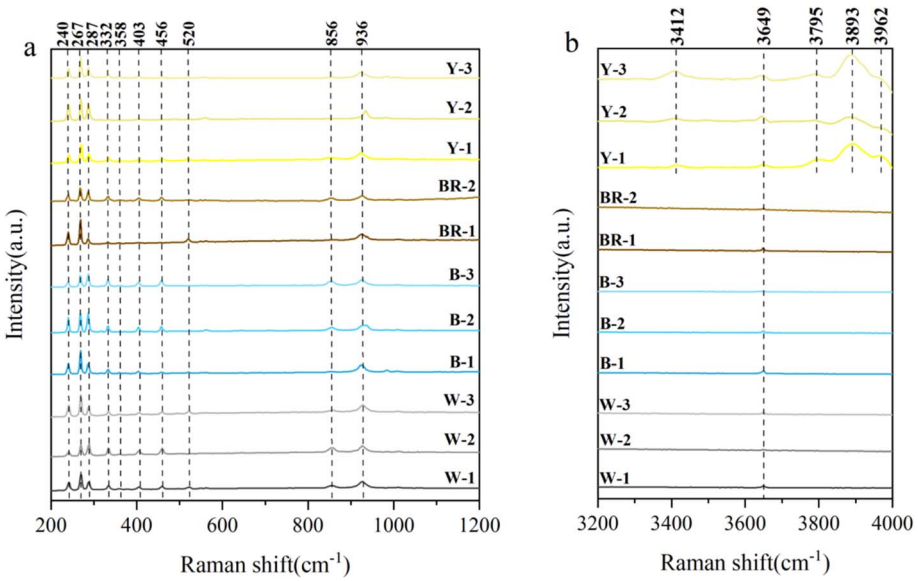

Fig. 6 (a) Raman spectra of the topaz samples (200–1200 cm^{-1}); (b) Raman spectra of the topaz samples (3200–4000 cm^{-1}).

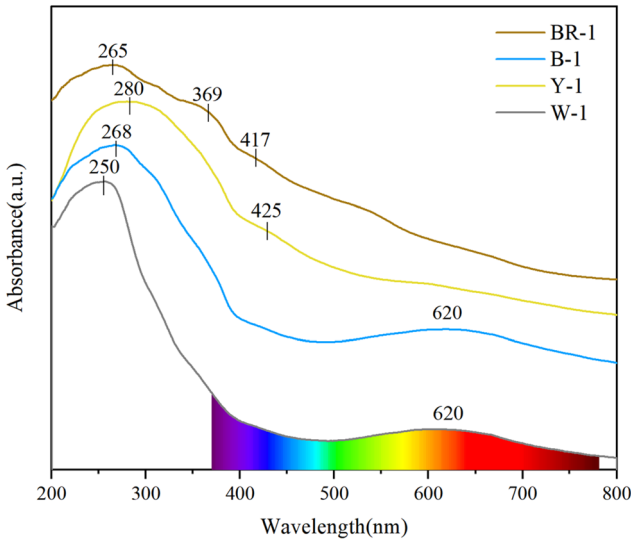

Fig. 7 UV-vis spectra of colorless, yellow, blue and brown topaz samples.

3.3.3. UV-vis spectra. To elucidate the coloration mechanism of natural topaz exhibiting various hues, we conducted an analysis of the ultraviolet-visible absorption spectrum, as presented in Fig. 7. The UV-vis spectra are plotted using Origin software from the raw data. We measured the absorption rate of the samples for light in the 200–800 nm spectral region by the reflection method, so the absorption is located at the peak. Table 5 lists the peak positions and peak assignments for the UV-vis spectra.

Each topaz sample exhibited significant absorbance in the 230–305 nm range, likely attributable to the Al═Si═O structure. This absorbance feature is also observed in spodumene.[31]

The coloration of yellow topaz is attributed to the absorption bands at 280 nm and 425 nm. The 280 nm absorption band is a combined effect of the $O^{2-} \rightarrow Fe^{3+}$ charge transfer and the Al═Si═O structure. In hydroxyl radicals, the O^{2-} serves as a ligand, and its lone pair of electrons undergoes a transition to the vacant d-orbitals of Fe^{3+}. This transition demands a relatively high energy and absorbs ultraviolet to violet light within the visible spectrum. The absorption band at 425 nm is caused by the $^6A_{1g} \rightarrow {}^4E_g + {}^4A_{1g}$ d–d electron transitions of Fe^{3+} (ref. 32) The combined effect of the $O^{2-} \rightarrow Fe^{3+}$ charge transfer and the $^6A_{1g} \rightarrow {}^4E_g + {}^4A_{1g}$ d–d electron transitions of Fe^{3+} is to absorb blue and violet light, causing topaz to display the complementary color of blue and violet light, that is, yellow. Furthermore, the intensity of the yellow color increases with higher concentrations of Fe.[14] The XRF analysis indicates that yellow topaz contains significantly higher levels of Fe compared to topaz of other colors, strongly supporting the proposed coloration mechanism. Meanwhile, the coloration mechanism explains the reason why yellow topaz is rich in hydroxyl groups, that is, the $O^{2-} \rightarrow Fe^{3+}$ charge transfer requires sufficient hydroxyl radical ligands. By synthesizing the features of low fluorine content (10.079 wt% average) and high hydroxyl concentration in yellow topaz, coupled with its coloration mechanism, we propose that the yellow coloration of topaz serves as a robust indicator of hydrothermal or metamorphic mineralization processes. It is probably linked to post-magmatic fluid activity, metamorphic dehydration, or hydrothermal alteration.[20]

The coloration of brown topaz is attributed to the small broad bands centered at 369 nm and 417 nm, which is different from the small broad band in the 460–480 nm range reported in previous studies.[33] The absorption at 369 nm is caused by the $^6A_{1g} \rightarrow {}^4T_{2g}$ d–d electron transitions of Fe^{3+} (ref. 32). The 417 nm absorption is attributed to a combination of trapped-electron and O^- centers, which are potential defect structures responsible for this spectral feature.[34,35] The combined effect of these two minor absorption bands results in topaz exhibiting a brown hue.

The coloration of blue topaz is related to a broad absorption band centered at 620 nm. This band has been attributed to the presence of Cr^{3+}, Fe^{2+}, and Mn^{2+} impurities by many authors.[2,36] Given the absence of Mn ions (Table 2) and discernible absorption signatures corresponding to Cr^{3+} and Fe^{2+} in blue topaz, the absorption band centered at approximately 620 nm can be deemed to originate from O^- centers.[37] We propose that by natural light irradiation, these O^- centers are formed by taking a hydrogen atom away from hydroxyl radicals OH^-. The liberated hydrogen atoms can form diamagnetic H_2 molecules or become immobilized through interactions with impurity sites.[9] The O^- centers can absorb light at specific wavelengths, creating an absorption band in the visible region, specifically forming a broad absorption band around 620 nm. This band

Table 5 Assignment of the UV-vis spectra of the topaz samples

Color type	Peak positions (nm)	Peak assignments[31,32,34,35,37]
Colorless	250	Al═Si═O structure
	620	O^- centers
Yellow	280	Combined effect of $O^{2-} \rightarrow Fe^{3+}$ charge transfer and Al═Si═O structure
	425	$^6A_{1g} \rightarrow {}^4E_g + {}^4A_{1g}$ d–d electron transitions of Fe^{3+}
Blue	268	Al═Si═O structure
	620	O^- centers
Brown	265	Al═Si═O structure
	369	$^6A_{1g} \rightarrow {}^4T_{2g}$ d–d electron transitions of Fe^{3+}
	417	Combination of trapped-electron and O^- centers

primarily absorbs orange light, resulting in the complementary color blue being exhibited by the topaz.

Notably, colorless topaz exhibits a broad absorption band centered at 620 nm, which contrasts with the absence of absorption bands in the visible light range reported in prior studies.[38] As colorless topaz contains only trace amounts of Mn ions and exhibits no absorption peaks for Cr^{3+} or Fe^{2+}, we conclude that the broad absorption band is also attributed to O^- centers. Previous studies have reported that the EPR spectra of natural colorless topaz and natural blue topaz are very similar, both characterized by a peak at $g = 2$ caused by the O^- centers. The only difference lies in the peak intensity, with the peak intensity at $g = 2$ in natural blue topaz being significantly higher than that in natural colorless topaz.[12] In addition, the absorption band at 620 nm correlates linearly with the EPR signal intensity of the O^- centers.[9] Therefore, we propose that the specific reason for the absence of coloration in natural colorless topaz, despite the presence of O^- centers, is likely attributed to an insufficient concentration of O^- centers to induce observable coloration.

Conclusions

This study is based on the investigation of the composition, structure and spectral characteristics of four different colors (colorless, yellow, blue and brown) of natural topaz, and through comparative analysis, their gemological and mineralogical characteristics and coloration mechanisms were concluded. The color of topaz is different because of the substitution of impurity ions for Al^{3+}, and the presence and concentration of color centers. The blue hue in natural topaz is due to a high concentration of O^- centers, which interact with two equivalent structural Al^{3+}. This interaction results in a stable blue color and causes a shift in the bending vibration peak position of the Al–O–Si bond in the infrared spectrum. Colorless topaz appears colorless because the concentration of O^- centers that it contains is too low to cause a change in its body color. Yellow topaz contains substantial Fe impurities, and the $O^{2-} \rightarrow Fe^{3+}$ charge transfer and the $^6A_{1g} \rightarrow {}^4E_g + {}^4A_{1g}$ d–d electron transitions of Fe^{3+} jointly contribute to the coloration of yellow topaz. Compared to topaz of other colors, yellow topaz exhibits a notably higher concentration of OH groups, and coupled with its coloration mechanism, we propose that the yellow coloration of topaz serves as a robust indicator of hydrothermal or metamorphic mineralization processes. Brown topaz is associated with the $^6A_{1g} \rightarrow {}^4T_{2g}$ d–d electron transitions of Fe^{3+} and a combination of trapped-electron and O^- centers. This study deepens the theoretical understanding of natural topaz coloration mechanisms and offers a robust experimental basis for elucidating its gemological and mineralogical characteristics. Additionally, it proposes a potential correlation between the yellow hue of topaz and its deposit genesis.

Data availability

All relevant data are within the manuscript.

Author contributions

Xin Zhang: data collection, analysis, writing the original draft; Nai Wang: review and editing, supervision; Yifan Gong: investigation. All authors have read and approved the final manuscript.

Conflicts of interest

The authors declare that they have no known competing financial interests or personal relationships that could have appeared to influence the work reported in this paper.

Acknowledgements

We would like to thank the laboratory of the School of Gemmology, China University of Geosciences, Beijing, for their help with this experiment. The authors are particularly grateful to Yujun Shi for his help in analyzing the experiment, and to Biao Yang for his support in the experiment.

References

1 G. D. Gatta, F. Nestola, G. Bromiley and A. Loose, *Am. Mineral.*, 2006, **91**, 1839–1846.
2 V. Skvortsova, N. Mironova-Ulmane, L. Trinkler and G. Chikvaidze, *IOP Conf. Ser.: Mater. Sci. Eng.*, 2013, **49**, 012051.
3 M. Pinheiro, C. Fantini, K. Krambrock, A. Persiano, M. Dantas and M. Pimenta, *Phys. Rev. B*, 2002, **65**, 104301.
4 P. Ribbe and G. Gibbs, *Am. Mineral.*, 1971, **56**, 24–30.
5 M. Pichavant and D. Manning, *Phys. Earth Planet. Inter.*, 1984, **35**, 31–50.
6 R. P. Taylor and A. E. Fallick, *Terra Nova*, 1997, **9**, 105–108.
7 R. Y. Zhang, J. G. Liou and J. F. Shu, *Am. Mineral.*, 2002, **87**, 445–453.
8 J. W. Howard, *J. Chem. Educ.*, 1935, **12**, 153.
9 D. d. Silva, K. Guedes, M. Pinheiro, J. Spaeth and K. Krambrock, *Phys. Chem. Miner.*, 2005, **32**, 436–441.
10 D. Da Silva, K. Guedes, M. Pinheiro, S. Schweizer, J. M. Spaeth and K. Krambrock, *Phys. Status Solidi C*, 2005, **2**, 397–400.
11 R. Bassoo, D. Eames, M. F. Hardman and K. Befus, *Gems Gemol.*, 2023, 59.
12 A. C. Dickinson and W. J. Moore, *J. Phys. Chem.*, 1967, **71**, 231–240.
13 M. Taran, A. Tarashchan, H. Rager, S. Schott, K. Schürmann and W. Iwanuch, *Phys. Chem. Miner.*, 2003, **30**, 546–555.
14 Z. Song, Q. Guo and L. Liao, *Crystals*, 2022, **12**, 1746.
15 C. Londos, A. Vassilikou-Dova, G. Georgiou and L. Fytros, *Phys. Status Solidi*, 1992, **133**, 473–479.
16 K. Komatsu, T. Kuribayashi and Y. Kudoh, *J. Mineral. Petrol. Sci.*, 2003, **98**, 167–180.
17 V. Correcher, J. Garcia-Guinea, C. Martin-Fernandez and N. Can, *Spectrosc. Lett.*, 2011, **44**, 486–489.
18 Y. Zheng, X. Yu and H. Guo, *Minerals*, 2019, **9**, 777.

19 M. A. Marks, H. R. Marschall, P. Schühle, A. Guth, T. Wenzel, D. E. Jacob, M. Barth and G. Markl, *Chem. Geol.*, 2013, **344**, 73–90.
20 M. Soufi, *Earth-Sci. Rev.*, 2021, **213**, 103467.
21 M. L. Frezzotti, S. Ferrando, L. Dallai and R. Compagnoni, *J. Petrol.*, 2007, **48**, 1219–1241.
22 G. R. Rossman, *Elements*, 2009, **5**, 159–162.
23 H. Sun, H. Li, N. J. Evans, H. Yang and P. Wu, *Ore Geol. Rev.*, 2017, **88**, 289–303.
24 V. C. Farmer, *The Infrared Spectra of Minerals*, Mineralogical Society, London, 1974, vol. 4, pp. 51–67.
25 J. A. Gadsden, *Infrared spectra of minerals and related inorganic compounds*, Butterworths, 1975.
26 K. Komatsu, H. Kagi, T. Okada, T. Kuribayashi, J. B. Parise and Y. Kudoh, *Am. Mineral.*, 2005, **90**, 266–270.
27 J. Beny and B. Piriou, *Phys. Chem. Miner.*, 1987, **15**, 148–159.
28 B. Wang and J. Tu, *Guang Pu Xue Yu Guang Pu Fen Xi*, 2000, **20**, 40–43.
29 S. Churakov and B. Wunder, *Phys. Chem. Miner.*, 2004, **31**, 131–141.
30 R. D. Aines and G. R. Rossman, *Am. Mineral.*, 1986, **71**, 1186–1193.
31 W. Bonventi Jr, S. Isotani and A. R. P. Albuquerque, *Adv. Condens. Matter Phys.*, 2012, **2012**, 873804.
32 H. Wang, Q. Guan, Y. Liu and Y. Guo, *Minerals*, 2022, **12**, 86.
33 R. Bassoo, D. Eames, M. F. Hardman, K. Befus and Z. Sun, *Gems Gemol.*, 2023, 59.
34 S. Schott, H. Rager, K. SCHÜRMANN and M. Taran, *Eur. J. Mineral.*, 2003, **15**, 701–706.
35 M. Gaft, R. Reisfeld and G. Panczer, *Modern Luminescence Spectroscopy of Minerals and Materials*, Springer, 2015.
36 V. Skvortsova, N. Mironova-Ulmane and L. Trinkler, *IOP Conf. Ser.: Mater. Sci. Eng.*, 2015, **80**, 012008.
37 K. Krambrock, L. Ribeiro, M. Pinheiro, A. Leal, M. d. B. C. Menezes and J.-M. Spaeth, *Phys. Chem. Miner.*, 2007, **34**, 437–444.
38 A. Ittipongse, A. Maneewong and I. M. W. Ekaputra, *Mater. Today: Proc.*, 2018, **5**, 15092–15097.